

PACS 07.60.Hv, 78.30.Jv, 85.60.Me, 87.80.+s

# A biosensor approach to probe the structure and function of the adsorbed proteins: fibrinogen at the gold surface

**B. A. Snopok\*, K. V. Kostyukevych, O. V. Rengevych,  
Y. M. Shirshov, E. F. Venger**

*Institute of Semiconductor Physics, NAS Ukraine, 45 prospekt Nauki, Kyiv, 252028, Ukraine*

*\* B.A.S.: Email: snopok@isp.kiev.ua; Telephone: +380 (44) 265 56 26; Phone (Voice&Fax): +380 (44) 265 18 27.*

**I. N. Kolesnikova, E. V. Lugovskoi**

*Palladin Institute of Biochemistry, NAS Ukraine, ul. Leontovicha 9, Kyiv-030, 252030 Ukraine*

**Abstract.** The kinetics of adsorption and surface structure of adsorbed layers of the human fibrinogen on the gold surface, determined by Surface Plasmon Resonance (SPR) and Atomic Force Microscopy (AFM) analysis, was employed to probe the lateral distribution and preferred orientation of protein molecules within the monolayer. In this study, special sets of immunoassays are presented for fibrinogen adsorption/conformation analysis. The results show that kinetic parameters of antigen-antibody interactions are directly related to the interfacial conformation of fibrinogen molecules. Various interfacial structures of adsorbed fibrinogen aggregates, namely single, bi- and three- molecular aggregates, were obtained using a combination of AFM imaging and SPR analysis. Adsorption of fibrinogen onto the surface of polycrystalline gold is a complex process including surface-induced unfolding, local self-assembly and adsorption, occurring concurrently with – and on the time scale of – each other. This result confirmed the utility of the proposed approach for detecting the spatial distribution and biofunctional properties of specific proteins adsorbed from biological liquids in biosensors.

**Keywords:** surface plasmon resonance, adsorbed proteins, fibrinogen, DD-fragment, E-fragment, biosensor, monoclonal antibodies, AFM, film chemistry control, polycrystalline gold films.

Paper received 10.10.98; revised manuscript received 10.10.98; accepted for publication 28.10.98.

## 1. Introduction

Formation and characterization of thin biofilms on solid substrates have been studied intensely for the past decade due to the potential for many technological applications, including biosensors [1-3]. In fact, understanding of the details of interactions between proteins and artificial surfaces is essential for many applications in medicine, biochemistry and ecology. In line with that, various concepts to control the specific adsorption of a particular protein and to prevent the nonspecific adsorption of other biological molecules onto different substrates have been extensively studied in order to understand the most favorable arrangement of surface-coupled receptor centers [4, 5]. At the same time, development of bioanalytical systems based on most promising adsorption biosensors requires taking into account a possible interfacial conformation of adsorbed molecules, which in turn can lead to deviations from the ideal behavior, and thus provide misleading results. Our continuing aim is to better

understand, at the molecular level, the adsorption mechanism and the peculiarities of interfacial transformation, so that we can develop optimal schemes to either inhibit or promote, as necessary, these adhesive reactions.

It is common knowledge that the first layer of biomolecules adsorbed onto a surface will undergo various degrees of conformational changes [6, 7]. As a result of these changes, new structures in the biomolecules will be formed, and the original surface will acquire new characteristics. To study the influence of a protein binding to a surface on their interfacial conformation and structure-function relationships of molecules at the interface, the interaction of fibrinogen with unmodified surface of thin gold films was chosen as a model system. Polycrystalline gold films were used as a substrate for this study since they are widely employed for various biosensor applications, and their surface chemistry is well-defined [8]. In addition, adsorption of proteins and other biomolecules on metal surfaces is often accompanied by chemical modification of the surface. Indeed, it has been shown that proteins tend to adjust its orientation and con-

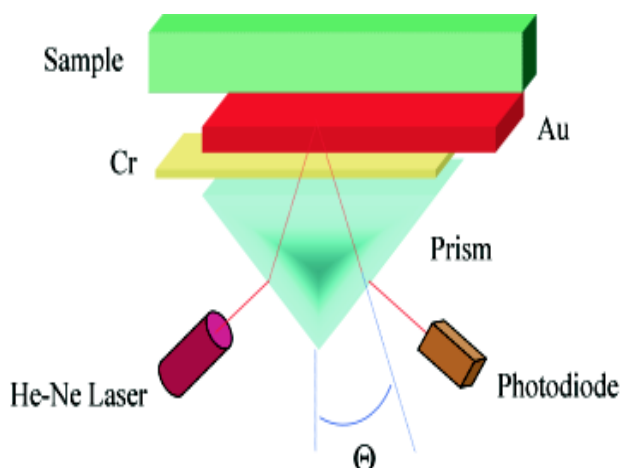
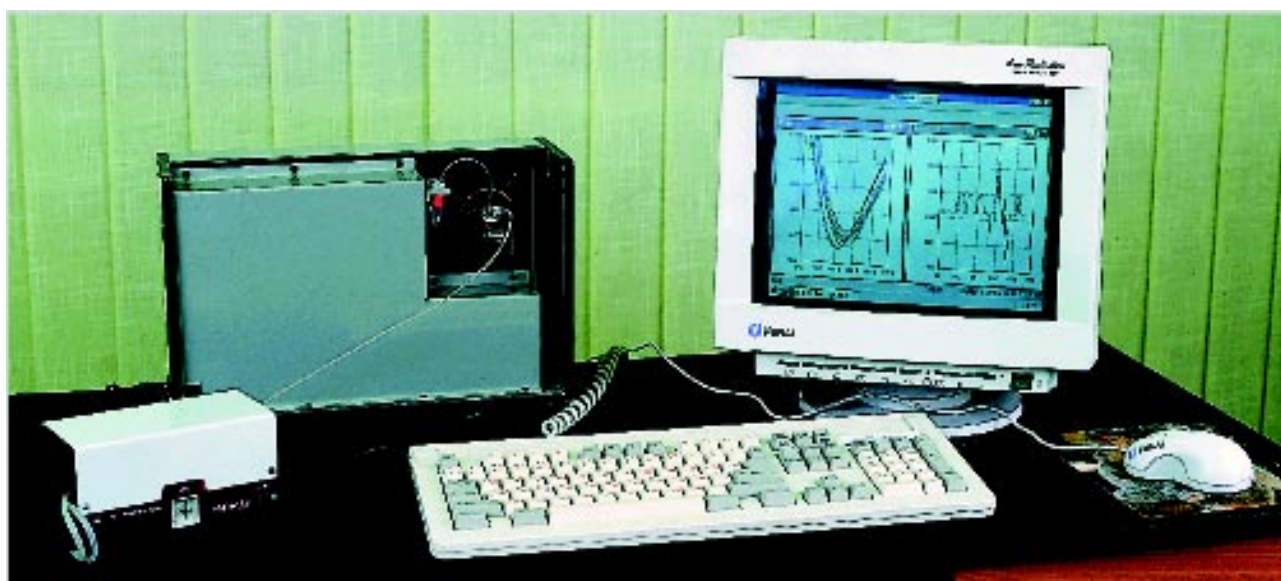


**Fig. 1.** General view (top) and schematic arrangement (bottom) of the components in the surface plasmon resonance analytical system *BioHelper PLASMON – 002*. The central element is the sensor chip mounted on the revolving table, which is driven by the stepper motor *via* the micrometer screw and the level arm.

formation on the surface of an artificial solid substrate, resulting in a stronger interaction at the interface and greater irreversibility of adsorption. Likewise, the fibrinogen, of all proteins in the plasma, adsorbs preferentially to various surfaces in a receptor-independent manner and can play a crucial role in biological phenomena accompanying clot formation [9]. So, in view of the need to characterize the real process on the surfaces of adsorption biosensors and develop the optimal strategies for ultimate control of the properties of artificial sensing surfaces, the peculiarities of both structure and function of adsorbed biomolecules invite further investigations.

A number of standard approaches have been advocated for analysis of protein adsorption [10, 11]. However, only a few of the existing analytical techniques can be used to study the binding process of unlabeled proteins in the real time mode. They are based on piezoelectric (*i.e.* gravimetric Quartz Crystal Microbalance and Surface Acoustic Wave [12, 13]) or evanescent wave (*i.e.* optical Surface Plasmon Resonance and waveguide spectroscopy [14, 15]) phenomena. Of particular importance to this work is combined use of surface plasmon resonance biosensor systems for analysis of protein adsorption on surfaces – atomic force

microscopy for surface characterization together with immunosensitive assays for biofunctional tests and exposure of structural peculiarities.

Immunosensitive analysis based on the polyclonal and monoclonal antibodies plays today an important role as a tool both for research and for routine analytical applications [17, 18]. In particular, changes in the affinity of the antibody can be used to detect modifications of the structure or function in one of the two immunological reactants (antigen or antibody). Obvious applications of this effect are, for instance, characterization of coupled antigens and control of their interfacial properties. For example, when attempts are made to measure the concentration of a protein with the help of adsorption biosensors, the best criterion to assess how closely the adsorbed protein matches the native one is to measure the comparative binding affinity of an antibody capable of reacting both with the free and adsorbed proteins.

Thus, the objective of our work was to study the fibrinogen adsorption onto untreated gold surface in order to understand how this surface influences the first biomolecular layer formed and how this first layer will adsorb additional biomolecules upon further contact with a biological fluid.

## 2. Theory of measurement

### Calculation of Adsorbed Protein Concentration

The surface concentration  $\Gamma$  (surface coverage) of proteins bound to the surface in units of mass/area (e.g. ng/mm<sup>2</sup>) can be calculated in terms of experimentally measurable quantities, such as the refractive index of the adsorbed layer and thickness within the adlayer in accordance with the approach proposed by de Feijter for homogeneous or inhomogeneous surface adlayers [19, 20]:

$$\Gamma = (dn_{\infty} / dc)^{-1} \cdot (n_s - n_1) \cdot d \quad (1)$$

where  $n_{\infty}$  is the refractive index of the protein at infinite distance from the surface,  $c$  – protein concentration,  $n_s$  and  $n_1$  – effective refractive indices of the adsorbed layer and solution, respectively, and  $d$  – mean thickness within the adlayer. Since in many practical situations the protein concentration in buffer solutions is extremely small, it is possible to assume that the refractive index of the protein solution is similar to that of the buffer solution. In this case, the surface coverage  $\Gamma$  can be calculated from the eq. 1, where  $n_1$  is substituted for buffer refractive index  $n_b$ . Applications of this approach to protein adsorption to the various surfaces have been presented repeatedly [21–23].

A simple and convenient way for determination of effective optical parameters and thicknesses of thin organic films is the surface plasmon resonance (SPR) method, which has been widely used to characterize thin organic films on metal surfaces [24, 25]. The key point is that a typical sensing distance from the surface into a dielectric medium for an SPR is of the order of 200 nm and consequently the effective change in refractive index directly corresponds to the adsorbed adlayers. In addition, SPR measurements can be performed in an *in situ* configuration and without any additional labels. However, despite the successful use of SPR techniques for characterization of various thin organic layers on metal surfaces, two points at issue require a special discussion – namely, discreteness of the monitoring characteristics of the SPR phenomena and correct calculation of the surface density of adsorbed proteins.

### Scanning SPR measurements

Surface plasmon resonance phenomena are collective electron oscillations in a metal causing electron density (charge density wave) fluctuations at the metal interface. In SPR scanning techniques employing the Kretschmann configuration [26], a *p*-polarized laser beam is directed onto the underside of a glass prism, the upper side being coated with a thin metal film with a negative real part of the dielectric permittivity (Ag, Au, etc.), and undergoes total internal reflection at the glass/metal interface (fig. 1). The reflectivity of a laser beam in this system is measured as a function of the incidence angle. The resulting response, denoted as SPR reflectivity curve, has several distinct features and can be quickly characterized by the position of the minimum (de-

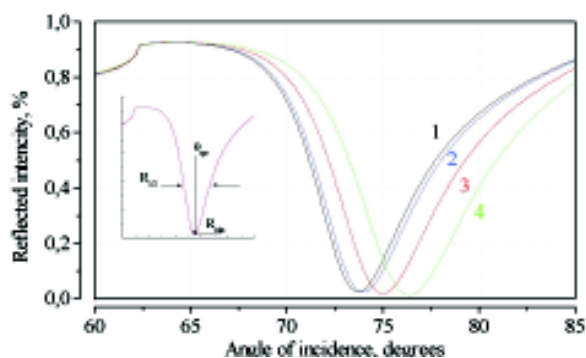


**Fig. 2.** Calculated reflectivity vs. angle of incidence scans for a model systems consisting semi-infinite glass prism ( $n_p = 1.515 + 0 \cdot i$ ), buffer solution ( $n_b = 1.337 + 0 \cdot i$ ), gold film ( $n_{Au} = 0.16 + 3.37 \cdot i$ , thickness 45 nm) and protein adlayer ( $n_s = 1.5 + 0 \cdot i$ ,  $d = 0$  nm - «1», 1 nm - «2», 5 nm - «3», 10 nm - «4»). The resonant excitation of the plasmon surface polaritons wave is seen in the reflectivity curve as a sharp dip at coupling angle  $\theta_{spr}$ .

noted as SPR angle  $\theta_{spr}$ ), the reflection value at the minimum ( $R_{spr}$ ) and the half-width ( $R_{1/2}$ ) (fig. 2). In several interpretations, these three parameters should result in determination of the complex dielectric permittivity and thickness of the layers in the system. Unfortunately, the exact analytical relation between the experimental values measured and the effective optical parameters of the system under consideration cannot be found in an analytical form from Fresnel's reflection equation [27], whereas numerical approximation for ultrathin films can lead to erroneous results [28]. To overcome the latter restriction, the two-wavelength configuration [29] or experimental procedure with measurements in different solvents [30] can be used, but these approaches are non-suitable for monitoring in real time. In addition, the classical Fresnel's theory does not take into account the physical effects complicating the SPR resonance response, such as light scattering and adsorption due to the surface roughness, scattering on volume defects etc., which can result in a non-predictable transformation of the resonance curve. Therefore, the techniques for determination of the refracting index and thickness based on the analysis of the resonance curve shape are very promising, but require further development.

At the same time, the SPR angle is a highly specific angle of incidence, attributed to the coupling between photons from the laser beam and surface plasmons at the outer metal interface. This coupling causes excitation of surface plasmons and subsequent reduction in the intensity of the internally reflected light, depends only on the dielectric properties of both the metal film and the layers above the sensor surface, and is not disturbed by the process of light scattering and optical absorption. Of particular importance for biosensor applications of SPR phenomena is adsorption of molecules from the solution on the chip surface that causes variations in the SPR angle, and hence the shift of  $\theta_{spr}$  can be employed

to detect the adsorption process on the surface in real time and without any additional labels.

To determine the relation of the SPR angle shift both to  $\Delta n_s = (n_s - n_b)$  and to  $d$ , one has to postulate a definite refractive index profile in the direction normal to the interface. The simplest approach is to consider a homogeneous adsorbed layer, with constant «optical» thickness  $d$  and mean refractive index  $n_s$ . For this simple situation, a common mathematical description for the relation between the reflectivity coefficient and the parameters of a multilayer structure is available [27]. Taking into consideration the difficulties of estimating from the analytical approximation the limits of validity for the final expression, we numerically calculated the relation between the shift of the SPR angle  $\theta_{spr}$  and  $\Delta n_s$  by using the so-called «method of Jones matrices» for different thicknesses [27, 31].

A model assuming two separate layers (gold film and adlayer) and two semi-infinite media (glass prism and liquid solution) represented the sensor chip. Each layer is defined by its thickness  $d_i$ , refractive index  $n_i$ , and extinction coefficient  $k_i$ . In the thin-film simulation program, the  $p$ -polarized reflectance is calculated as a function of the incident angle using complex Fresnel calculations. In the calculations, it is assumed that the interfaces between the layers are flat and the layers are homogeneous and isotropic. The distribution of adsorbed molecules within the adlayer was described as a random one with a constant thickness of the

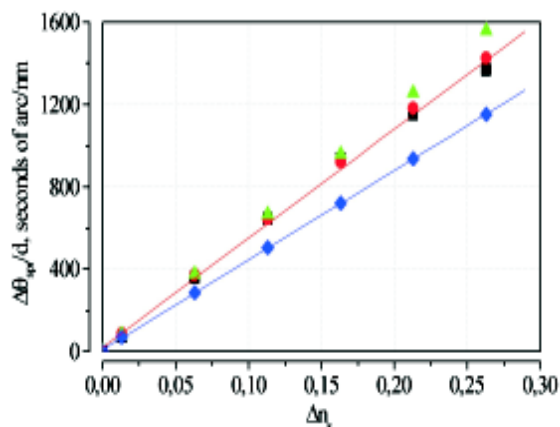


**Fig. 3.** Simulated set of the normalized shift of the SPR angle ( $\Delta\theta_{spr} = (\theta_{spr}^{adlayer} - \theta_{spr}^{gold})/d$ ) versus the deviation of the mean refractive index of adlayer's  $\Delta n_s$  at different  $d$  (1 - ■, 5 - ●, 10 - ♦). The sensor chip was represented by a model system consisting semi-infinite glass prism ( $n_p = 1.515 + 0 \cdot i$ ), gold film ( $n_{Au} = 0.16 + 3.37 \cdot i$ , thickness 45 nm), adlayer ( $n_s = (1.337 + \Delta n_s) + 0 \cdot i$ ,  $d$ , where  $\Delta n_s = (n_s - n_b)$ ) and semi-infinite buffer solution ( $n_b = 1.337 + 0 \cdot i$ ). The red solid line is the best linear fit of the average of several simulated curves for different adlayer thicknesses  $d$  and can be written as  $\Delta\theta_{spr} = 5300 \cdot \Delta n_s \cdot d$ . The blue solid line is the best linear fit of the simulated data for  $d = 1$  nm,  $n_{Au} = 0.16 + 3.6 \cdot i$  and can be written as  $\Delta\theta_{spr} = 4350 \cdot \Delta n_s \cdot d$ .

layer and effective mean refractive index. Since the deviation of the adlayer's refractive index is restricted by the value of the refractive index of the solvent (usually water solutions with the refractive index higher than 1.33) and organic solid films (generally with the mean refractive index lower than 1.6), the calculation was made in the range from 1.3 to 1.6 for  $n_s$  at different thicknesses of the layer ( $d = 1 - 15$  nm). Fig. 3 shows the calculated SPR response as a function of the mean refractive index deviation  $\Delta n_s$  from the PbS refractive index of 1.337 for a set of layers with thickness from 1 to 10 nm. Linear fitting of the data obviously reveals a linear dependence of the normalized shift of the SPR angle ( $\Delta\theta_{spr} = (\theta_{spr}^{adlayer} - \theta_{spr}^{gold})/d$ ) on deviation of the mean refractive index of the adlayer  $\Delta n_s$ , which may be expressed in a simple analytical form:

$$\Delta\theta_{spr} = K \cdot \Delta n_s \cdot d \quad (2)$$

where  $K$  is a conversion constant,  $\Delta\theta_{spr}$  is measured in arc seconds, and  $d$  – in nm.

#### Determining Conversion Constant

For reliable calculations of the surface concentration of analyte bound to the surface from the SPR response, it was necessary to determine separately the thickness of the gold layer and optical constants of the prism, gold layer and liquid medium. The glass prism and the liquid are semi-infinite, and the refractive indices (1.515 and 1.337, respectively) were determined with a refractometer. Thickness of the metal film (45 nm) was estimated by ellipsometry. At the same time, perfect determination of the effective optical constants of the metal film in a series of experiments is very difficult, since characteristics of vapor-deposited gold films may have slight differences due to noncontrolled disturbances during the fabrication process.

In order to understand the influence of minute changes in the parameters of sensor chips on the value of the conversion constant, we calculate the relation of  $K$  to  $n_{Au}$  and  $k_{Au}$  using the approach described above. It was shown that  $K$  depends on the  $n_{Au}$  very weakly in the range from 0.1 to 0.2, whereas the dependence of  $K$  on  $k_{Au}$  dependence in the range from 3 to 4 is exponential. Thus, for correct determination of  $K$  the accurate value of  $k_{Au}$  must be obtained, whereas the value of  $n_{Au} = 0.16$  estimated by ellipsometry can be used without additional corrections.

To determine the exact effective value of  $k_{Au}$ , experiments with a standard SPR chip were made in solutions with different values of the refractive index (water-glycerol mixtures). Using the measured values of  $\Delta\theta_{spr}$  shift amounting to 1739 arc seconds for a 5% mixture and 3720 arc seconds for 10% - water-glycerol solutions (relative to pure water), the corrected value of  $k_{Au} = 3.37$  was obtained, which is slightly different from the ellipsometry data (3.6). So, for a sensor chip represented by a model consisting of a semi-infinite glass prism ( $n_p = 1.51 + 0 \cdot i$ ), gold film ( $n_{Au} = 0.16 + 3.37 \cdot i$ , thickness 45 nm), adlayer ( $n_s + 0 \cdot i$ ,  $d = 1 - 10$ , where  $n_s = n_{buffer} + \Delta n_s$  and  $n_{buffer} = 1.337$ ) and semi-infinite buffer solution ( $n_b = 1.337 + 0 \cdot i$ ) the value of conversion

constant  $K$  is *ca.* 5300 seconds of arc/nm. It must be emphasized that despite the small variation of  $k_{Au}$  determined by SPR and ellipsometry (3.37 and 3.6 correspondingly), considerable differences was observed for the values of  $K$  (5300 and 4350 seconds of arc/nm, respectively) (fig.3).

Finally, the surface concentration for the adsorbed molecules can be calculated from the SPR data in accordance with the following expression:

$$\Gamma = (dn_{\infty}/dc)^{-1} \cdot (\Delta\theta_{spr}/5300) \quad (3)$$

where the refractive index increment for proteins is assumed to be constant up to high concentrations, as shown by de Feijter *et al.* [19]. Since the refractive index increment does not vary essentially with the kind of protein [20], we assume for all proteins used in this study the mean value of  $0.188 \text{ cm}^3 \cdot \text{g}^{-1}$ .

### 3. Materials and methods

#### *Surface Plasmon Resonance Sensor System*

The SPR system *BioHelper* PLASMON-002 designed by the Institute of Semiconductor Physics (ISP NASU, Kiev, Ukraine) was described in detail elsewhere [32]. Briefly, the light beam from the He-Ne laser ( $\lambda = 632.8 \text{ nm}$ ) is deflected by a mirror to the prism with a sensitive layer mounted on the revolving table, which can be rotated with a step motor connected to a micrometer screw with a lever arm. The position of the step motor is monitored by software with respect to the hardware reference point. A photodiode detector is positioned at the opposite side of the prism to monitor the laser light which is undergoes full internal reflection in the sensor chip. For a complete scan (*ca.*  $15^\circ$ ), the table must move from the left-most to the right-most position and back again, which takes about 15 s. A «track minimum» scan employed to analyze binding and dissociation kinetics lasts *ca.* 2 s. The experiments were controlled with an IBM-compatible computer running special software under Microsoft Windows. The peristaltic pump allows flow of solutions through the experimental cell, which is formed of silicone rubber covered with a Teflon holder and is mounted directly on the sensor chip surface. The cell has a round cross-section of *ca.*  $25 \text{ mm}^2$  in the direction perpendicular to the prism surface, height of more than 1 mm, and a volume of *ca.*  $25 \mu\text{l}$ .

#### *The SPR Sensor Chip Design*

The chip support is a trapezium-shape glass (K-8) prism of dimensions  $18 \times 12 \times 6 \text{ mm}$  and inclination angle of  $68^\circ$ . The refractive index of the prism is 1.515. For sensor formation, sputtered on the upper side of the support prism was a *ca.* 5 nm adhesive layer of Cr, followed by 45 nm of Au. During the deposition, the prism was kept at  $T = 22^\circ\text{C}$ , and then for three hours in high vacuum ( $5 \cdot 10^{-4} \text{ Pa}$ ) before removing from the evaporation equipment (VUP-5M).

Sensor chips were used for measurements without any additional cleaning procedures prior to the experiment. Untreated chips were mounted in the system and flushed with the buffer until the baseline drift was less than  $\pm 30$  angle seconds. All subsequent reaction steps were conducted in Phosphate buffered Saline (PbS), pH 7.2, at the ambient temperature of  $(20 \pm 2)^\circ\text{C}$ .

#### *Surface Analysis*

We used the contact mode of AFM imaging due to our interest to the irreversibly bounded protein. The AFM analysis confirmed the presence of the strongly adsorbed fibrinogen on the gold surface, whereas the AFM probe during imaging easily swept it on the surface of methyl-terminated dodecylthiol monolayers ( $\text{HS}(\text{CH}_2)_{11}\text{CH}_3$ , data not shown).

AFM imaging was performed using a commercial Nanoscope IIIa (Digital Instrument, Santa-Barbara) equipped with a 80- $\mu\text{m}$  scanner. The original SPR chips were used for the AFM analysis. The scans were performed in the contact force mode employing commercially available AFM tips made of silicone nitride with a scan frequency of approximately 1 Hz. Ellipsometry experiments were made on Au coated glass slides with a LEF-3M Ellipsometer (LOMO, St-Petersburg) at a  $70^\circ$  angle from the normal direction, using a He-Ne (632,8 nm) laser.

#### *Chemicals and Reagents*

*Human fibrinogen* was prepared from human plasma by sodium sulfate precipitation [33].

*DD fragment of fibrin* was prepared by plasmin hydrolysis of cross-linked fibrin. The DD fragment was isolated from lisate on fibrin agarose by the technique described by V. A. Belitzer *et al* [34]. The pure DD fragment was eluted and dialyzed against 0,05 M ammonium acetate buffer pH 8,5 and lyophilized.

*Fragment E<sub>3</sub>* was obtained by plasmin hydrolysis of fibrin clots completely cross-linked by factor XIIIa. Fragment E<sub>3</sub> was isolated from lisate on G-150 column (Pharmacia Sweden) equilibrated with 1,5 N potassium sulfocyanate in phosphate buffered saline (pH 7,2). Fragment E<sub>3</sub> was concentrated, dialyzed against water (pH 8,1) and lyophilized [35].

*Preparation of monoclonal antibodies (mAb)*. BALB/c mice were immunized intraperitoneally with 100 $\mu\text{g}$  N-terminal disulfide knots (N-DSK) of fibrinogen and with 100 $\mu\text{g}$  DD-fragment in Freund's complete adjuvant and then twice at 1-month intervals with 100 $\mu\text{g}$  in incomplete Freund's adjuvant. Two months after the third immunization, the mice were injected intraperitoneally with 100  $\mu\text{g}$  N-DSK and DD-fragment 3 days before fusion. Fusion of spleen cells from the immunized mice with myeloma X63-Ag8 cells was carried out with 50 % polyethylene glycol of 3 kDa. Growth and selection media were as described by Lerner [36].

The antibody was purified from cell culture media by affinity chromatography on protein G-Sepharose or Fibrinogen-Sepharose.

mAb's specificity was determined by solid indirect and competitive enzyme-linked immunosorbent assay (ELISA) with fibrinogen, fibrin, fragment E<sub>3</sub>, DD, N-DSK.

mAb's II-3B of IgG 1 classes, II-4d, II-1c and IV-2d of IgG 2A class react with DD-fragment of fibrin, fibrinogen, fibrin and D-monomer fragment.  $K_D$  value of the binding of mAb II-3B to DD -  $0,75 \cdot 10^{-9}$  M, II - 4d -  $2,8 \cdot 10^{-9}$  M.

mAb 2d-2a of IgG 1 class react with fibrinogen ( $K_D = 1,0 \cdot 10^{-9}$  M) and do not react with fibrin.

Purity of the samples of fibrinogen, E<sub>3</sub> -, DD-fragment and mAb's was studied by electrophoresis (SDS, PAAG), and specificity of mAb's – by immunoblotting.

### Sample Preparation

All protein solutions were made in PbS solution (pH 7.2) immediately prior to the analysis.

## 4. Results and discussion

The initial discussion focuses on the AFM characterization of the adsorbed layers of fibrinogen on the gold surface. In the next section, *in situ* investigations of both fibrinogen adsorption and its subsequent interactions with monoclonal antibodies are described in detail. The final section discusses possible adsorption mechanisms and peculiarities of the interfacial fibrinogen structure.

### The topography and interfacial structure of irreversibly adsorbed fibrinogen on an untreated gold coated prism

The gold-coated SPR prisms were initially imaged by AFM to characterize the native surface. The AFM image in fig. 4 shows that the surface is not atomically smooth, with the grain diameter of the gold coating ranging from 20 to 30 nm. The surface roughness shows a maximum height variation of 2.5 nm for a 500 nm scan, with the area root-mean-square (rms) surface roughness *ca.* 0.84 nm.

In order to fabricate a fibrinogen-based biofilm on the untreated gold surface, typical adsorption experiments were made (see below). The AFM results, depicted in fig. 4, clearly show that under the adsorption conditions employed in this study, a fibrinogen concentration of  $73 \mu\text{g}\cdot\text{ml}^{-1}$  in PbS solution was sufficient to achieve a smooth continuous film. The surface roughness shows a maximum height variation of above 1 nm for a 500 nm scan, with an area rms of *ca.* 1.2 nm. An increase in the bulk concentration of fibrinogen does not change essentially the surface topography as well as rms (0.9 nm at  $300 \mu\text{g}\cdot\text{ml}^{-1}$  bulk concentration). It was also shown that as the concentration of fibrinogen in solution decreased, the number of defects and holes in the fibrinogen layer increased (data not shown). The average thickness of the fibrinogen film determined by both AFM (above 6.5 nm, fig. 5) and ellipsometry (above 7.6 nm with the refractive index of fibrinogen set to 1.5) had similar values.

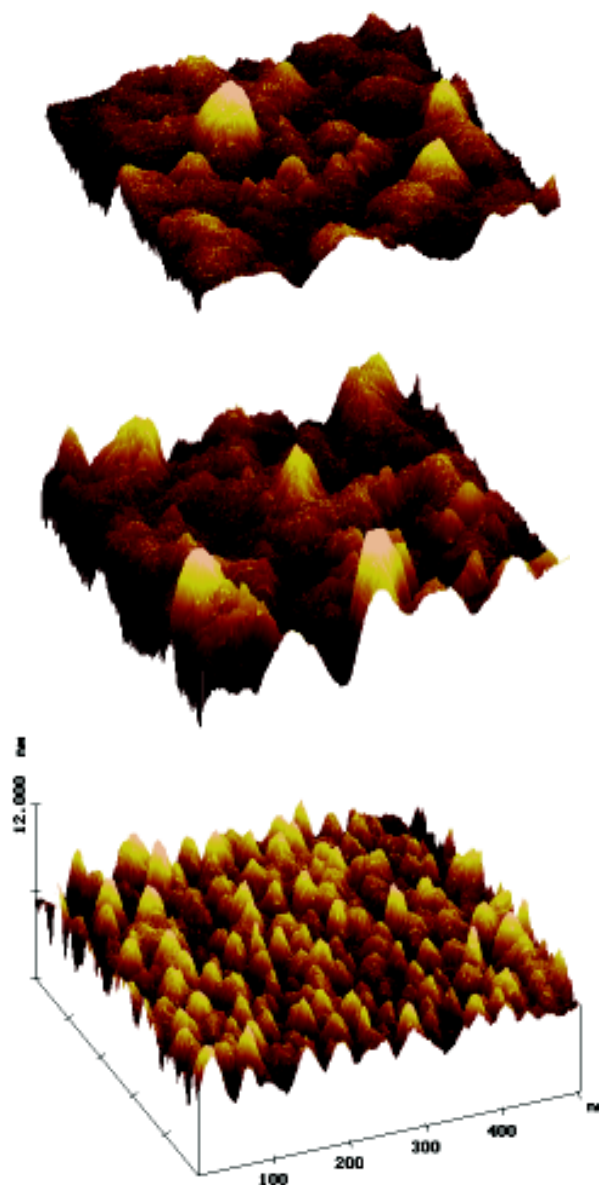


**Fig. 4.** An atomic force microscope image (500 nm square scan) of the untreated gold surface of an SPR sensor chip (bottom) and AFM images of fibrinogen films cast from  $73 \mu\text{g}\cdot\text{ml}^{-1}$  (middle) and  $600 \mu\text{g}\cdot\text{ml}^{-1}$  (top) solution concentration onto unmodified gold SPR microprism.

The AFM images of the fibrinogen coated surfaces shown in fig. 4 resolve features which are consistent with protein molecular structure. Indeed, as results from comparative analysis of the Power Spectral Densities (PSD, [37]) function (fig. 6) of AFM images of untreated gold and fibrinogen film, the surface of adsorbed fibrinogen has distinctive surface objects with linear dimensions of *ca.* 90 and 140 nm, that can not be fit into individual molecules of fibrinogen.

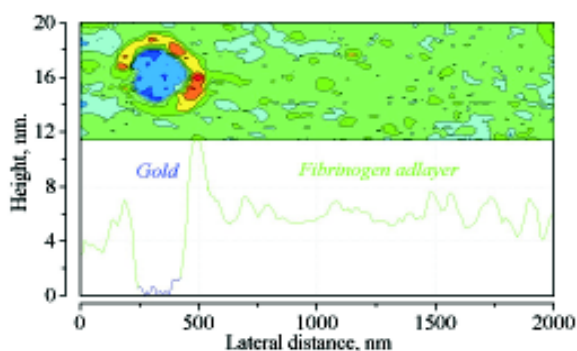


**Fig. 5.** Section (bottom) of an AFM image (top) of fibrinogen film cast from  $300 \mu\text{g}\cdot\text{ml}^{-1}$  solution concentration onto unmodified gold SPR prism with the area of nonmodified gold surface. The estimated value of fibrinogen film thickness is *ca.* 6 nm.

Formation of separate islands with the height up to *ca.* 10 nm has been observed for partially formed layers adsorbed from fibrinogen solution in PbS with the concentration lower than  $20 \mu\text{g}\cdot\text{ml}^{-1}$ . Three types of objects with different structures have been extracted from these images, which are shown in fig. 7. The highly pronounced double-humped shape of the top aggregate with longitudinal length of *ca.* 140 nm evidently correlates with a similar value obtained from PSD analysis of continuous films for the statistically dominating distinctive surface element. Moreover, a dome-shaped surface objects with lateral dimensions *ca.* 90 nm are observed as well. Taking into consideration relatively large dimensions of this object, it is possible to suggest that this observation may result from some kind of local self-organization of the fibrinogen molecules. To study the internal structure of such aggregates, additional information about the molecular structure of fibrinogen molecule is required.

The structure of fibrinogen (molecular weight is *ca.* 340 000 Da) has been repeatedly discussed based on the results of various indirect investigations [38–40], since X-ray crystallography of fibrinogen is impossible because of the non-crystalline solid state of this protein. However, fibrinogen has been imaged using both electron microscopy and AFM [41, 42], showing it to have a triad structure of length 45 nm with central (E) domain (*ca.* 5 nm diameter) and two distal (D) domains elongated to approximately 10 nm by 6 nm.

Thus, AFM analysis combined with information about spatial dimensions of fibrinogen molecules enabled us to make the following suggestions about the possible structure of the surface objects observed, depicted in fig. 7. The bottom picture in fig. 7 can correspond to partly unfolded fibrinogen molecules. The domelike shape and dimensions of *ca.* 90 nm of the object shown in the middle picture are in a good agreement with the assumption that it is a bimolecular aggregate of fibrinogen with face-to-face reciprocal

arrangement of D-fragments of fibrinogen molecules. The most probable explanation of the origin of the aggregate shown in the top picture is formation of fibrinogen three-molecule aggregate in halfstaggered overlapping manner with association of the molecules in the direction of their long axis like natural fibrin filaments. Possible intrinsic structure and potential orientation of the unfolded, bi- and three-associated fibrinogen aggregates at the surface of thin polycrystalline gold films are pictured schematically in fig. 7.

We cannot completely rule out our early assumption about formation of fibrinogen dimers in a halfstaggered overlapping manner followed by association of the dimers in the direction of their perpendicular long axis at low fibrinogen concentration in solutions [43]. This suggestion was based on the fact that the width of the aggregates is *ca.* 60–70 nm and similar to the length of the fibrinogen dimer formed in a halfstaggered overlapping manner. However, in our opinion, it is unlikely for several reasons: (1) it is well known that broadening of molecular features on AFM images can be caused by tip-induced effects [44]; (2) this model cannot explain the existence of fixed surface aggregates with a different shape and (3) the stability of bi-molecular aggregate with reciprocal arrangement in halfstaggered overlapping manner is not obvious because the second recognition center in central E-domain remains open for coupling of additional fibrinogen molecules. Since AFM imaging provides only topographic information about the protein surface, more complete and correct understanding of the surface properties of protein biofilm requires additional information about the peculiarities of the surface function.

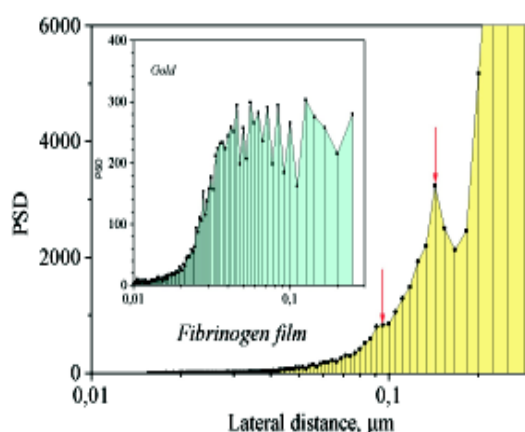


**Fig. 6.** Two - dimensional Power Spectral Densities functions for untreated gold surface and fibrinogen film cast from  $300 \mu\text{g}\cdot\text{ml}^{-1}$  solution concentration onto unmodified gold SPR micropism. At the fibrinogen surface, the PSD function reveals periodic surface features which might otherwise appear «random». Most powerful waveform is detected at *ca.* 140 nm, corresponding to the dominant waveform of the image. Additional periodic structure is detected at shorter wavelengths (*ca.* 90 nm).

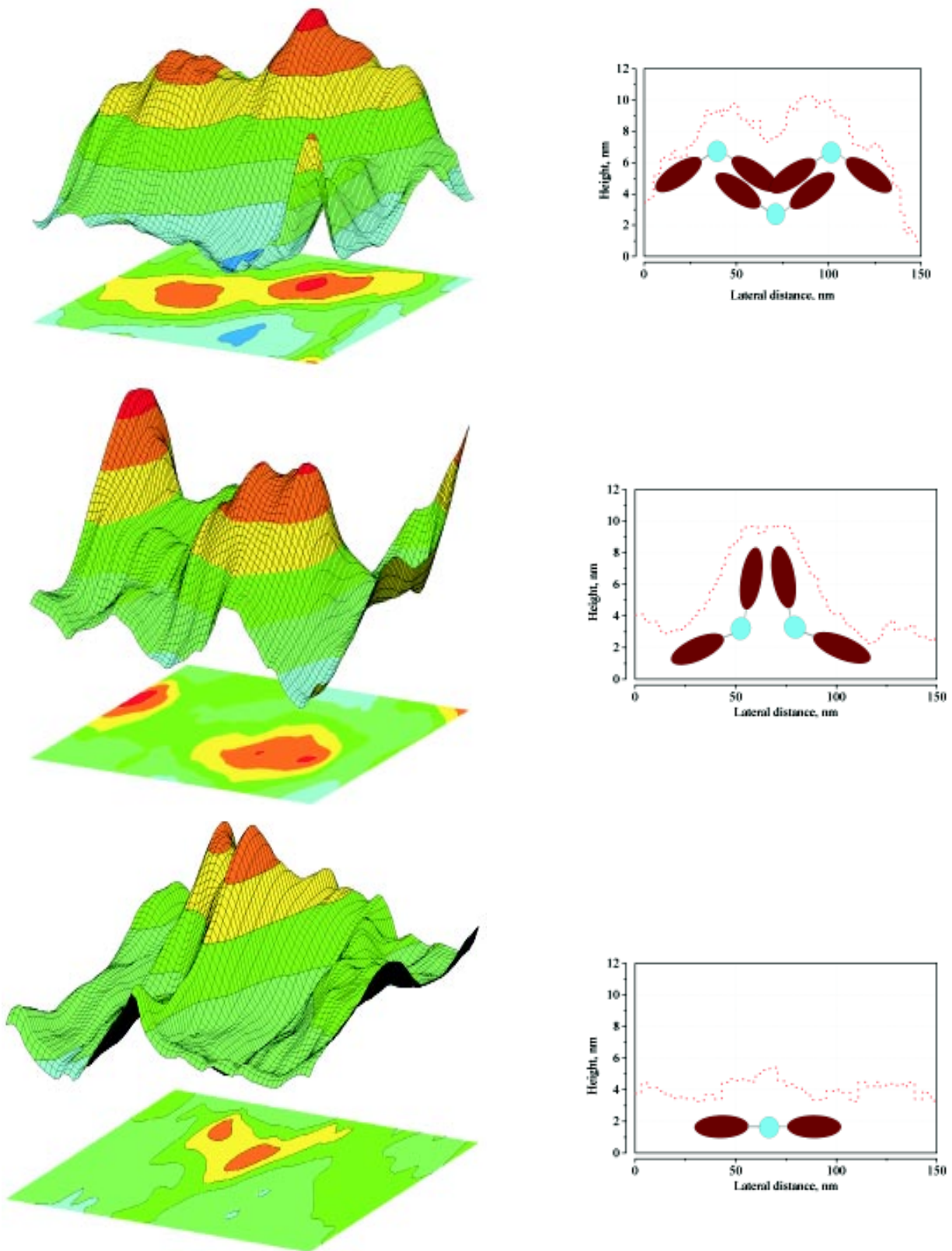


**Fig. 7.** Typical fibrinogen aggregates at the the surface of thin polycrystalline gold films and their possible intrinsic structure: single (botton), bi- (middle) and three- (top) molecules fibrinogen aggregates. AFM fragments (125×125 nm) obtained from AFM images (500×500 nm) of fibrinogen films cast from 9.3  $\mu\text{g}\cdot\text{ml}^{-1}$  solution concentration onto unmodified gold SPR microprism.

*Fibrinogen adsorption to untreated gold-coated prism: SPR analysis*

In order to illustrate the reproducibility of the SPR system using the unmodified SPR microprism, a typical fibrinogen adsorption experiment was undertaken in quintuple. The PbS buffer was allowed to flow through the cell and then sharply substituted with the protein solution. After the sensor response reached an equilibrium state without flow, the protein solution was again replaced by PbS. Results of these experiments with injection of a portion of fibrinogen solution in PbS with concentration of  $73 \mu\text{g}\cdot\text{ml}^{-1}$  are shown in fig. 8. It is seen that the SPR angle increases with fibrinogen adsorption to a plateau value and gives rise to an SPR shift of  $4750 \pm 250$  seconds of arc after an extended time period (*ca.* 800 s). It is necessary to stress that no additional loosely bounded molecules from the sensor surface were removed during washing by pure PbS.

The surface coverage of adsorbed fibrinogen layer formed at the bulk concentration of  $73 \mu\text{g}\cdot\text{ml}^{-1}$  is *ca.*  $5 \text{ ng}\cdot\text{mm}^{-2}$ , which is more essential than that for the «side-on» orientation of fibrinogen at the interface. Indeed, simple estimations of the surface coverage for fibrinogen adlayer in «side-on» adsorption manner assuming an ellipsoidal shape of molecule and lateral dimensions of 45 nm by 6 nm, results in  $\Gamma$  approximately of  $2 \text{ ng}\cdot\text{mm}^{-2}$ . Such a result is in excellent agreement with the previous assumption, those surface transformations involve not only the unfolding process, but also some local self-organization with various arrangement of molecules on the surface.

In order to understand the nature of the limiting step in the fibrinogen adsorption onto gold surface, namely irreversible surface coupling, the kinetic analysis of fibrinogen, its DD- and E-fragment was investigated quantitatively. The kinetics of adsorption of these proteins were employed to probe the location of the site, which is predominantly

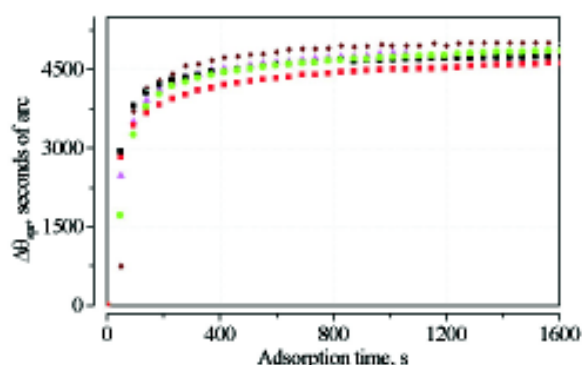


**Fig. 8.** Adsorption of fibrinogen from PbS solution with concentration of  $73 \mu\text{g}\cdot\text{ml}^{-1}$  to unmodified gold surface of five different sensor chips. Saturation was reached after approximately 800 sec. The mean value of SPR angle shift is  $4750 \pm 250$  seconds of arc (*ca.*  $5 \text{ ng}\cdot\text{mm}^{-2}$ ).

*ΦKO, 1(1), 1998*  
*SQO, 1(1), 1998*

binding to gold. Taking into consideration a high concentration of disulfide bonds in E-fragment combined with its spherical shape and relatively small size, it was suggested that irreversible surface coupling of fibrinogen includes at the first step an interaction between the gold surface and E-fragment of fibrinogen. As long as the relative affinity of molecules to the surface can be estimated from the rate of adsorption of the corresponding proteins, at a similar mass flow from the bulk to the surface, the experimental charts has been approximated by the equation [45]:

$$\Gamma = \Gamma_{\max} \cdot (1 - \exp(-k \cdot t^{1/2})) \quad (4)$$

where  $k$  is a rate constant (fig. 9). It can be seen that the rates of adsorption for both fibrinogen and its DD-fragment are very similar ( $0.05$  and  $0.07 \text{ s}^{-1/2}$  correspondingly) and more small one for E-fragment ( $> 0.2 \text{ s}^{-1/2}$ ). Such a result is entirely consistent with the proposal that the first step of irreversible fibrinogen adsorption can be determined by binding of E-fragment to the gold surface.

From the SPR adsorption profiles in fig. 9 it appears that all three proteins adsorb to the surface until saturation and without any «loosely» bounded molecules (data not shown). However, there is a difference in the equilibrium SPR angle for the three proteins in order of increasing value: E-fragment ( $1571$ ) < DD-fragment ( $2165$ ) < fibrinogen ( $2777$  seconds of arc), which does not directly correspond to the molecular weights of this molecules (*ca.*  $50\,000$ ,  $190\,000$  and  $340\,000 \text{ Da}$  correspondingly). These findings may be explained by considering the molecular dimensions of the protein and their potential conformation at the gold/solution interface.

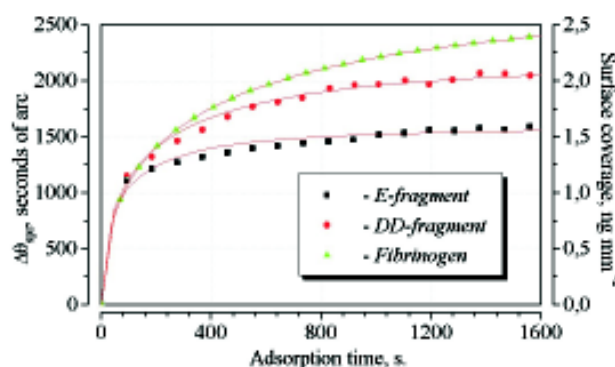


**Fig. 9.** Adsorption of fibrinogen, E-fragment and DD-fragment of fibrinogen from PbS solution with concentration of  $25 \mu\text{g}\cdot\text{ml}^{-1}$  to the unmodified gold surface. Nonlinear regression analysis (applying eq. (4):  $\Gamma = \Gamma_{\max} \cdot (1 - \exp(-k \cdot t^{1/2}))$ ) gives the following solution: for fibrinogen –  $\Delta\theta_{\max}^{Fb} = 2780$  seconds of arc,  $\Gamma_{\max}^{Fb} = 2.79 \text{ ng}\cdot\text{mm}^{-2}$ ,  $k_{\text{eff}}^{Fb} = 0.05 \text{ s}^{-1/2}$ , for DD-fragment –  $\Delta\theta_{\max}^{DD} = 2170$  seconds of arc,  $\Gamma_{\max}^{DD} = 2.18 \text{ ng}\cdot\text{mm}^{-2}$ ,  $k_{\text{eff}}^{DD} = 0.07 \text{ s}^{-1/2}$ , for E-fragment –  $\Delta\theta_{\max}^E = 1350$  seconds of arc,  $\Gamma_{\max}^E = 1.36 \text{ ng}\cdot\text{mm}^{-2}$ ,  $k_{\text{eff}}^E = 0.23 \text{ s}^{-1/2}$ .

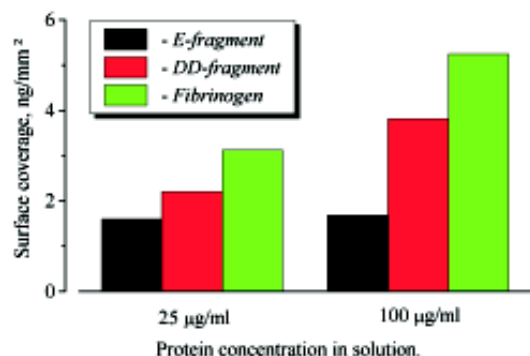


**Fig. 10.** Surface coverage of fibrinogen, DD-fragment and E-fragment at the surface of unmodified gold films *versus* bulk concentration of proteins in PbS.

An attempt was made using the SPR method to determine the role of a different fragment of fibrinogen in the processes of surface induced transformations of protein structure. In line with this, the influence of protein concentration in solution on the total mass of the adsorbed layer as measured by SPR was investigated and is shown in fig. 10 for solutions with a concentration of 25 and 100 µg·ml<sup>-1</sup>. The results show that the level of adsorption increases with solution concentration for both fibrinogen and its DD-fragment, whereas the equilibrium angle shift values are not significantly different for E-fragment of fibrinogen. This observation is consistent with formation of an adsorbed monolayer of E-fragment from native, non-unfolded molecules in the wide range of protein concentration in solution. At the same time, the results suggest that both fibrinogen and its DD-fragment undergo conformational transformations at the surface of untreated gold films at a low protein concentration in the solution. Thus, the spatial structure of adsorbed molecules of fibrinogen and its DD - fragment at the gold surface is different from that in the native form. Moreover, the relation of the total adsorbed mass of proteins to their concentration in the solution is similar for fibrinogen and its DD-fragment. In view of the non-unfolded adsorbed form of E-fragment, this fact permits suggesting that unfolding of

fibrinogen, for the most part, is determined by the conformational transformations in the D-domains. To account for this, we hypothesized, first, that the fibrinogen exists on the gold surface in a partly denatured, non desorptionable form, and, second, that denaturation of this protein is surface-induced process, occurring concurrently with adsorption.

In agreement with previous studies of fibrinogen [46, 47], it is shown *in situ* that no additional fibrinogen adsorbs on the first fibrinogen adlayer. Evaluation of the interaction between adsorbed both E- and DD-fragments shows a similar behavior. At the same time, DD fragment was found to bind moderately to E-adlayer, but no binding with fibrinogen adlayer was observed. The saturated SPR angle shift values for all possible situations are tabulated in Table 1. We should note an avid binding of fibrinogen to E-adlayer with saturated surface coverage similar to one at the unmodified gold surface.

*The study of biochemical status of adsorbed fibrinogen with immunoassays*

To get more insight into the mechanism of fibrinogen adsorption and to study the possible ways of conformational transformation and probable orientation of proteins at the surface of untreated gold films, special immunoassays for binding of fibrinogen using monoclonal antibodies against different epitops in the fibrinogen molecules were developed. Thus, two set of immunoassays for both N-terminated (mAb 2d-2a vs epitop in E-domain) and C-terminated (mAbs 2-1c, 2-3b, 2-4d and 4-2d vs epitops in D-domain) portions of fibrinogen chains using monoclonal antibodies were developed.

Four kind of monoclonal antibodies against the D-fragment of the fibrinogen molecules were used to study the conformational alteration of the molecules on the gold surface. The localization of the epitopes for the antibodies and the study of their interactions with adsorbed fibrinogen allow us to conclude that only part of epitopes in the D-fragment conserve their native conformation and point toward the solution (fig. 11). It must be emphasized that binding of the monoclonal antibody directed vs. different epitops in the C-terminated portions of fibrinogen chains shows a notable value of selective interactions with fibrinogen adlayers, that was not simply dependent on the total amount of adsorbed fibrinogen but rather on its conformation. In general, it is

**Table 1.** Adsorption of fibrinogen (73 µg·ml<sup>-1</sup>), DD-fragment (25 µg·ml<sup>-1</sup>), and E-fragment (25 µg·ml<sup>-1</sup>), onto surface of fibrinogen, DD-fragment and E-fragment biofilm.

Solution / Adsorbed	Fibrinogen ( $\Delta\theta_{spr}/\Gamma$ ) second of arc \ ng·mm <sup>-2</sup>	DD-fragment ( $\Delta\theta_{spr}/\Gamma$ ) second of arc \ ng·mm <sup>-2</sup>	E-fragment ( $\Delta\theta_{spr}/\Gamma$ ) second of arc \ ng·mm <sup>-2</sup>
Fibrinogen	0	0	560\0.56
DD-fragment	1430\1.44	0	0
E-fragment	3600\3.61	880\0.88	0

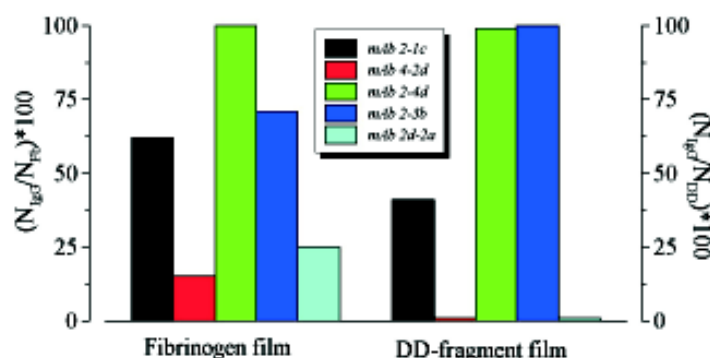


**Fig. 11.** Interactions of monoclonal antibodies with fibrinogen film cast from  $73 \mu\text{g}\cdot\text{ml}^{-1}$  solution concentration and DD-fragment of fibrinogen cast from  $25 \mu\text{g}\cdot\text{ml}^{-1}$  solution concentration onto unmodified gold SPR microprism.  $N^{\text{mAb}}/N^{\text{Fb/DD}}*100$  is calculated from the saturated value of SPR shift and molecular weight  $W$  of proteins:  $N^{\text{mAb}}/N^{\text{Protein}} = (\Delta\theta_{\text{max}}^{\text{mAb}}/\Delta\theta_{\text{max}}^{\text{Protein}}) \times (W^{\text{Protein}}/W^{\text{mAb}})$ .

possible to conclude that, despite a similar behavior of mAb's on both fibrinogen and DD-fragment surface, the spatial structure of adsorbed fibrinogen is more in line with the native form of protein.

As would be expected, the mAb 2d-2a vs. N-terminated portion of fibrinogen chains do not interact with adsorbed DD-fragment. At the same time, the interaction of mAb 2d-2a with fibrinogen adlayer yields surface coverage of  $0.55 \text{ ng}\cdot\text{mm}^{-2}$ , which corresponds approximately to 25–30 % of the total number of adsorbed fibrinogen molecules. So, it is possible to assume that the above 30 % of biofunctional fibrinogen molecules have orientation at the interface with N-terminated disulfide knots of E-fragment pointed in solution.

The total amount of the biofunctional adsorbed fibrinogen molecules can be estimated from the experiments with mAb's 2-4d and 2-3b, those interaction with adsorbed both fibrinogen and DD-fragment are in similar manner and in above 1:1 fashion. Taking into consideration, that each of molecules either fibrinogen or DD-fragment have two identical epitops for those mAb's and different packing inside the monolayer, simple one-to-one interaction testifies that approximately 50 % of adsorbed molecules retain their biofunctional properties. So, the number of the N-terminated disulfide knots of fibrinogen which maintain their biofunctional properties and are recognized by mAb 2d-2a results in approximately 60 % of total number of biofunctional molecules. Such a result is gratifyingly consistent with previous studies by AFM imaging, where it was assumed that the dominant surface aggregate has two from three E-fragments pointing to the solution. These results, together with the fact of irreversible coupling of protein films to the sensor surface, do not contradict to our suggestion that fibrinogen molecules bind to the gold surface with disulfide bonds after their splitting in the central E – domain.

Another experiment with mAb's against epitops in D- and E-domains of fibrinogen was performed to probe the

orientation of the adsorbed fibrinogen on the surface treated by E-fragment. The immunosensitive analysis of fibrinogen adsorption on the surface of adsorbed E-fragment shows that the surface orientation of fibrinogen molecules corresponds to inaccessibility of E-fragment of fibrinogen molecules for monoclonal mAb (2d-2a). So, in this case, all E-fragments of adsorbed fibrinogen molecules directed to the surface of adsorbed E-fragment.

#### *General model of fibrinogen adsorption onto the surface of polycrystalline gold films*

The mechanism suggested here for protein adsorption is an extension of the classic reaction-diffusion mechanism which is followed by a wide variety of physical phenomena depending on the protein concentration in solution [48, 49]. The first step of fibrinogen adsorption is considered to be reversible and adsorbed molecules have uniform distribution at the surface. At the next step, proteins undergo surface transitions, changing from «loosely» bound to «irreversibly» bound due to coupling between gold and E-fragment of fibrinogen. We suggest that activation of the polymerization sites in adsorbed fibrinogen molecules occurs at this step. Formation of primary fibrinogen dimers could be increased at this step due to the interactions of D-fragments of fibrinogen, whereas formation of primary three-molecular aggregates is determined by the classical biophysical mechanism of «polymerization» in fibrin-like manner [50]. Formation of the latter type of aggregate is a self-terminated process provided by blocking of the polymerization active sites in extreme D-fragments by gold surface. The contribution of either kind of surface aggregate dictates both steric requirements for each mechanism and possible free area. In addition, one can suppose that the specific structure of untreated polycrystalline gold surface with «mountains» and «valleys» may result in capturing predominantly the E-fragment of fibrinogen owing to the steric restrictions. Indeed, a small size of E-domain combined with flexible bridges between it

and a peripheral D-domain can support the requirement of spatial conformation of fibrinogen molecules at the non-flat gold surface. Such special reciprocal arrangement of domain structure of fibrinogen together with possible splitting of disulfid bonds in E-domain can result in a strong, irreversible adsorption of fibrinogen on the gold surface. Ultimately, the final structure of the adsorbed layer depends on the relation between rate constant of these processes (namely, unfolding, self-aggregation and adsorption) and could be changed by means of increasing/decreasing the fibrinogen concentration in the solution.

## 5. Concluding remarks

Controlling irreversible protein adsorption to surfaces is a major concept for nearly every biological assay or sensor and is of equal importance for this model fibrinogen-based system. We describe here the use of a surface plasmon resonance biosensor system that allows kinetic measurements of native non-labeled biomolecules, to study the peculiarities of protein adsorption onto untreated gold surface and interactions of monoclonal antibodies with their irreversibly binding layers. A notable feature of the technique is ability to distinguish a possible influence of substrate chemistry on the adsorption processes, which may be related to changes in the surface orientation or packing density within the monolayer.

The adsorption of three proteins, fibrinogen, its DD- and E-fragments onto unmodified gold surface of polycrystalline gold films and subsequent their adlayers interactions with monoclonal antibodies against different epitops in native molecules has been studied by means of Surface Plasmon Resonance biosensor instrument as a model system for structural and functional analysis of protein biofilm. It was shown based on the combined use of AFM imaging and SPR kinetic analysis that fibrinogen adsorption onto gold surface is a complex process including at least three different mechanisms: surface-induced unfolding, local self-assembly and adsorption, which are occurring concurrently with – and on the time scale of – each other. Unfolding of the protein at the gold surface results in a decrease of the number of adsorbed molecules which retain their biofunctional properties (approximately 50 % of total adsorbed mass). At the same time, the local self-assembling process leads to formation of the special molecular aggregates whose structure depends on the primary arrangement of adsorbed molecules. The rate of adsorption, controlled for the most part by the mass flow from the bulk solution, determines the contribution both self-assembling and unfolding.

Thus, the combined application of the immunoassay-based SPR analysis with the molecular resolution imaging of the AFM provides a significant insight into the formation mechanism and interfacial properties of the artificial biomolecular structures at various interfaces.

## 6. Acknowledgements

This work was concluded with the partial financial support of the INCO-COPERNICUS (project PL 965131).

## References

1. M. Malmsten, *Biopolymers at interfaces*, Marcel Dekker, Inc. (1998).
2. S. Lofas, M. Malmqvist, I. Ronnberg, E. Stenberg, Bo Liedberg and I. Lundstrom, *Bioanalysis with surface plasmon resonance*, *Sensor and Actuators*, B **5**, pp. 79-84 (1991).
3. Yu. M. Shirshov, V. I. Chegel, Yu. V. Subbota, A. E. Rachcov, T. A. Sergeeva, Determination of polarizability and surface concentration of biomolecules using surface plasmon resonance experiment, *SPIE Proc.*, **2648**, pp. 118-123 (1995).
4. S. Spinke, M. Liley, F. J. Schmitt, H. S. Guder, L. Angermaier, W. Knoll, Molecular recognition at self-assembled monolayers: optimization of surface functionalization, *J. Chem. Phys.*, **99**, pp. 7012-7019 (1993).
5. F.-J. Schmitt, L. Haussling, H. Ringsdorf, W. Knoll, Surface plasmon studies of specific recognition reactions at self-assembled monolayers on gold, *Thin Solid Films*, **210-211**, pp. 815-817 (1992).
6. G. S. Retzinger, B. C. Cook, A. P. Deanglis, The binding of fibrinogen to surfaces and the identification of two distinct surface-bond species of the protein, *J. Colloid Interface Sci.*, **168**, pp. 514-521 (1994).
7. J. E. Lee and S. S. Saaverda, Molecular orientation in heme protein films adsorbed to hydrophilic and hydrophobic glass surfaces, *Langmuir*, **12**, pp. 4025-4032 (1996).
8. L.-H. Guo, J. S. Facci, G. McLendon, r. Mosher, Effect of gold topography and surface pretreatment on the self-assembly of alkanethiol monolayers, *Langmuir*, **10**, pp. 4588-4593 (1994).
9. E. W. Salzman, E. W. Merrill, *Hemostasis and thrombosis: basic principles and clinical practice*, Lippincott, Philadelphia (1987).
10. D. G. Myszka, Kinetic analysis of macromolecular interactions using surface plasmon resonance biosensors, *Current Opinion in Biotechnology*, **8**, pp. 50-57 (1997).
11. R. Karlsson, H. Roos, L. Fagerstam, and B. Persson, Kinetic and concentration analysis using BIA technology, *Methods: A companion to methods in enzymology*, **6**, pp. 99-110 (1994).
12. Y. Ebara, K. Itakura, Y. Okahata, Kinetic studies of molecular recognition based on hydrogen bonding at the air-water interface by using a highly sensitive quartz-crystal microbalance, *Langmuir*, **12**, pp. 5165-5170 (1996).
13. A. J. Ricco, R. M. Crooks, G. C. Osbourn, Surface acoustic wave chemical sensor arrays: new chemically sensitive interfaces combined with novel cluster analysis to detect volatile organic compounds and mixtures, *Acc. Chem. Res.*, **31** (5), pp. 289-295 (1998).
14. R. J. Green, J. Davies, M. C. Davies, C. J. Roberts and S. J. B. Tendler, Surface plasmon resonance for real time in situ analysis of protein adsorption to polymer surfaces, *Biomaterials*, **18**, pp. 405-413 (1997).
15. A. Bernard and H. R. Bosshard, Real-time monitoring of antigen-antibody recognition on a metal oxide surface by an optical grating coupler sensor, *Eur. J. Biochem.*, **230**, pp. 416-423 (1995).
16. A. C. Malmborg, A. Michaelsson, M. Ohlin, B. Jansson, C. A. K. Borrebaeck, Real time analysis of antibody-antigen reaction kinetics, *Scand. J. Immunol.*, **35**, pp. 643-650 (1992).
17. A. Horenstein, C. Poiesi, M. Camagna, L. de Monte, M. Mariani, A. Albertini, F. Malavasi, Biosensor analysis of antigen-antibody interactions a priority step in the generation of monoclonal bispecific antibodies, *Cell Biophysics*, **24/25**, pp. 109-117 (1994).
18. P. End, I. Gout, M. J. Fry, G. Panayotou, R. Dhand, K. Yonezawa, M. Kasuga, M. D. Waterfield, A biosensor approach to probe the structure and function of the p85a subunit of the phosphatidylinositol 3-kinase complex, *J. Biol. Chem.*, **268** (14), pp. 10066-10075 (1993).
19. J. A. de Feijter, J. Benjamins and F. A. Veer, Ellipsometry as a tool to study the adsorption behaviour of polymers at the air-water interface, *Biopolymers*, **17**, p. 1759 (1978).
20. D. Clerc, W. Lukosz, Integrated optical output grating coupler as refractometer and (bio-) chemical sensor, *Sensor and Actuators*, B **11**, pp. 461-465 (1993).
21. M. Malmsten, J.-A. Johansson, N. L. Burns, H. K. Yasuda, Protein adsorption at n-butane plasma polymer surfaces, *Colloids and Surfaces B: Biointerfaces*, **6**, pp. 191-199 (1996).
22. R. Reiter, H. Motschmann, W. Knoll, Ellipsometric characterization of streptavidin binding to biotin-functionalized lipid monolayers at the water/air interface, *Langmuir*, **9**, pp. 2430-2435 (1993).

23. V.Razumas, T.Nylander, T.Arnebrant, An ellipsometric and electrochemical study of microperoxidase-8 and-11 adsorption on platinum and gold surfaces, *J. Colloid Interface Sci.*, **164**, pp. 181-189 (1994).
24. A.G.Frutos and R.M.Corn, SPR of ultrathin organic films, *Anal. Chem. News & Features*, **70**, pp. 449A-455A (1998).
25. W.Knoll, Optical characterization of organic thin films and interfaces with evanescent waves, *MRS Bulletin*, **16** (7), pp. 29-39 (1991).
26. E.Kretschmann, Die bestimmung optischer konstanten von metallen durch anregung von oberflachen plasmaschwingungen, *Z.Phys.*, **241** (4), pp. 313-324 (1971).
27. R.M.A. Azzam, N.M.Bashara, Ellipsometry and polarized light, North-Holland, Amsterdam (1977).
28. S.R. Wasserman, G.M.Whitesides, I.M.Tidswell, M.Ocko, P.S.Pershan, J.D.Axe, *J.Am.Chem.Soc.*, **111**, pp. 5852-5861 (1989).
29. R.L.Earp, R.E.Dessy, Surface plasmon resonance, Wiley Publishing (1997).
30. G.V.Beketov, Y.M.Shirshov, O.V.Shynkarenko, V.I.Chegel, Surface plasmon resonance spectroscopy: prospects of superstrate refractive index variation for separate extraction of molecular layer parameters, *Sensor and Actuators, B*, **48**, pp. 432-438 (1998).
31. S.A.Kostioukevich, Yu.M.Shirshov, E.P.Matsas, A.V.Stronski, Yu.V.Subbota, V.I.Chegel, P.E.Shepelyavi, Application of surface plasmon resonance for the investigation of ultrathin metal films, *SPIE Proc.*, **2648**, pp. 144-151 (1995).
32. K.V.Kostioukevich, B.I.A.Snopok, S.A.Zinio, Y.M.Shirshov, I.N.Kolesnikova, E.V.Lugovskoi, New opto-electronic system based on the surface plasmon resonance phenomenon: application to the concentration determination of DD-fragment of fibrinogen, *SPIE Proc.*, p. 3414 (1998).
33. T.V.Varetskaya, Mikroheterogeneity of fibrinogen. Cryofibrinogen, *Ukrainskii Biokhemicnii Zhurnal*, **32**, pp. 13-24 (1960) (in Ukrainian).
34. V.A.Belitzer, T.M.Pozdniakova, T.P.Ugarova, Light and heavy fractions of fragment D: preparation and examination of fibrin binding properties, *Thromb.Rev.*, **19**, pp. 807-814 (1980).
35. S.A.Olexa, A.Z.Budzynski, R.F.Doolittle, B.A.Cottrell, Th.S.Greens, Structure of fragment E species from human cross-linked fibrin, *Biochemistry*, **20**, pp. 6139-6145 (1981).
36. B.H.Lerner, How to make a hibridoma, *Yale Jornal of Biology and Medicine*, **54**, pp. 387-402 (1981).
37. J.C.Stover, Optical scattering: measurement and analysis, McGraw-Hill, Inc.(1990).
38. T.M.Pozdniakova, Mechanism fibrin self-assembled, *Biohimia jivotnih i cheloveka*, **13**, pp. 27-36 (1989) ( in Russian).
39. L.V. Medved, S.V. Litvinovich, Multidomen structure molecule of fibrinogen, *Biohimia jivotnih i cheloveka*, **13**, pp. 18-27 (1989) (in Russian).
40. E.V.Lugovskoi, E.M.Makogonenko, V.S.Chudnovets, S.G.Derzskaya, G.K.Gogolinskaya, I.N.Kolesnikova, A.M.Bukhanevich, I.N.Sitak, E.D.Lyashko, S.V.Komissarenko, The study of fibrin polymerization with monoclonal antibodies, *Biomedical science*, **2**, pp. 249-256 (1991).
41. R.F.Doolittle, Fibrinogen and fibrin, *Ann. Rev. Biochem.*, **53**, pp. 195-229 (1984).
42. R.Wigren, H.Eluring, R.Erlandsson, S.Welin, I.Lundstrom, Structure of adsorbed fibrinogen obtained by scanning force microscopy, *FEBS*, **280**, pp.225-228 (1991).
43. Y.Shirshov, B.Snopok, K.Kostioukevich, E.Shinkarenko, I.Gavriluk, I.Kolesnikova, E.Lugovskoi, S.Komissarenko, Fibrinogen at the gold surface: peculiarities of the adsorption kinetic and film structure, *Proc. ECOF*, **7**, pp. 393-395, Potsdam, Germany (1998).
44. I.Schmitz, M.Scheiner, G.Friedbacher, M.Grasserbauer, Tapping-mode AFM in comparison to contact-mode AFM as a tool for in situ investigations of surface reactions with reference to glass corrosion, *Anal. Chem.*, **69**, pp. 1012-1018 (1997).
45. K.A.Peterlinz and R.Georgiadis, In situ kinetics of self-assembly by surface plasmon resonance spectroscopy, *Langmuir*, **12**, pp. 4731-4740 (1996).
46. M.Malmsten, Ellipsometry studies of protein adsorption at lipid surfaces, *J. Colloid Interface Sci.*, **168**, pp. 247-254 (1994).
47. M.Malmsten, B.Lassen, Competitive adsorption at hydrophobic surfaces from binary protein systems, *J. Colloid Interface Sci.*, **166**, pp. 490-498 (1994).
48. C.F.Lu, A.Nadarajan, K.K.Chittur, A comprehensive model of multiprotein adsorption on surfaces, *J.Colloid Interface Sci.*, **168**, pp. 152-161 (1994).
49. V.P.Zhdanov, B.Kasemo, Monte Carlo simulations of the kinetics of protein adsorption, *Surf. Rev. Lett.*, **5** (2), pp. 615-634 (1998).
50. Yu.A.Ovchinnikov, Bioorganic chemistry, M: Prosveshenie (1987).

## БІОСЕНСОРНИЙ ПІДХІД ДО ВИВЧЕННЯ СТРУКТУРИ ТА ФУНКЦІОНУВАННЯ АДСОРБОВАНИХ БІЛКІВ: ФІБРИНОГЕН НА ЗОЛОТІЙ ПОВЕРХНІ

**Б. А. Снопок, К. В. Костюкевич, А. В. Ренгевич, Ю. М. Ширшов, Є. Ф. Венгер**  
 Інститут фізики напівпровідників НАН України

**І. Н. Колеснікова, Е. В. Луговський**  
 Інститут біохімії ім. А. В. Паладіна НАН України

Просторовий розподіл та переважна орієнтація молекул білків у моношарі досліджена з застосуванням кінетики поверхневого плазмонного резонансу (ППР) та мікроскопії атомних сил (МАС) підчас адсорбції фібриногену людини на поверхню золота. У роботі проведена серія специфічних імунних реакцій щоб проаналізувати адсорбційно-конформаційний стан плівок фібриногену. Отримані результати демонструють прямий зв'язок кінетичних параметрів реакції антиген-антитіло з конформацією фібриногену на межі розподілу. Застосування МАС і ППР аналізів дало можливість визначити одно-, двух- та трьох молекулярні структурні сполуки фібриногену на межі розподілу. Адсорбція фібриногену на поверхню полікрісталічного золота - це складний процес, що містить: розгортання, стимульоване поверхнею, само-збирання та адсорбцію, які відбуваються конкурентно у часі. Цей результат підтверджує перспективу запропонованого підходу у біосенсорній техніці для визначення просторового розподілу та біофункціональних властивостей специфічних білків, які адсорбуються з біологічних рідин.

**БИОСЕНСОРНЫЙ ПОДХОД К ИЗУЧЕНИЮ СТРУКТУРЫ И ФУНКЦИИ АДсорБИРУЕМЫХ БЕЛКОВ: ФИБРИНОГЕН НА ПОВЕРХНОСТИ ЗОЛОТА**

*Б. А. Снопок, К. В. Костюкевич, А. В. Ренгевич, Ю. М. Шишов, Е. Ф. Венгер  
Институт физики полупроводников НАН Украины*

*И. Н. Колесникова, Е. В. Луговский  
Институт биохимии им. А. В. Палладина НАН Украины*

Пространственное распределение и преимущественная ориентация молекул белков в монослое изучена с использованием кинетики поверхностного плазмонного резонанса (ППР) и микроскопии атомных сил (МАС) при адсорбции фибриногена человека на поверхность золота. В работе проведена серия специфических иммунных реакций для адсорбционно-конформационного анализа пленок фибриногена. Полученные результаты демонстрируют прямую связь кинетических параметров реакции антиген-антитело с конформацией фибриногена на границе раздела. Применение МАК и ППР анализов позволило определить одно-, двух и трех-молекулярные сочетания фибриногена на границе раздела. Адсорбция фибриногена на поверхность поликристаллического золота является сложным процессом, включающим, разворачивание, стимулируемое поверхностью, само-сборку и адсорбцию, происходящим конкурентно во времени. Этот результат подтверждает перспективу предлагаемого подхода в биосенсорной технике для определения пространственного распределения и био-функциональных свойств специфических белков, адсорбируемых из биологических жидкостей.